

LETTERS

A turbulent wake as a tracer of 30,000 years of Mira's mass loss history

D. Christopher Martin¹, Mark Seibert², James D. Neill¹, David Schiminovich³, Karl Forster¹, R. Michael Rich⁴, Barry Y. Welsh⁵, Barry F. Madore², Jonathan M. Wheatley⁴, Patrick Morrissey¹ & Tom A. Barlow¹

Mira is one of the first variable stars ever discovered¹ and it is the prototype (and also the nearest example) of a class of low-to-intermediate-mass stars in the late stages of stellar evolution. These stars are relatively common and they return a large fraction of their original mass to the interstellar medium (ISM) (ref. 2) through a processed, dusty, molecular wind. Thus stars in Mira's stage of evolution have a direct impact on subsequent star and planet formation in their host galaxy. Previously, the only direct observation³ of the interaction between Mira-type stellar winds and the ISM was in the infrared. Here we report the discovery of an ultraviolet-emitting bow shock and turbulent wake extending over 2 degrees on the sky, arising from Mira's large space velocity and the interaction between its wind and the ISM. The wake is visible only in the far ultraviolet and is consistent with an unusual emission mechanism whereby molecular hydrogen is excited by turbulent mixing of cool molecular gas and shock-heated gas. This wind wake is a tracer of the past 30,000 years of Mira's mass-loss history and provides an excellent laboratory for studying turbulent stellar wind–ISM interactions.

Mira is a binary system with an orbital period⁴ of ~500 years. The primary star, Mira A, is the luminous, mass-shedding, evolved star that exhibits long-period, semi-regular variability. These properties arise because Mira A has exhausted the supply of hydrogen and helium in its core and at present is powered by helium and hydrogen fusion in a shell surrounding a carbon–oxygen core. These physical conditions typify what are known as asymptotic giant branch (AGB) stars. The secondary star, Mira B, is much less luminous and is usually classified as a white dwarf, but this is somewhat controversial^{5,6}. The orbital distance is so large that only a small fraction of the wind from Mira A is accreted by Mira B. Any outflow from Mira B, although potentially fast, is probably insignificant both from the perspective of mass flux and from the energetics compared to Mira A.

During routine inspection of incoming images taken with the GALEX ultraviolet satellite⁷, we noticed a nebulosity near the position of Mira. We obtained the deeper images shown in Figs 1 and 2, displaying a bow-shock-like feature south of Mira and a nebulosity extending northward in a comet-like structure spanning a total length of two degrees (see Supplementary Information for additional figures). Adopting the revised Hipparcos-based distance⁸ to Mira of 107 pc, the tail has a physical size of 4 pc. The direction of the tail is consistent with Mira's proper motion⁹ of $d(\alpha, \delta)/dt = (-28, -224) \text{ mas yr}^{-1}$ (corrected for solar motion), where α is right ascension, δ is declination and t is time. The appearance of a bow shock is consistent with Mira's large space velocity of $v_0 = 130 \text{ km s}^{-1}$, which we calculate from the proper motion and the radial velocity¹⁰ of $+63 \text{ km s}^{-1}$. Thus, the tail traces the extrapolated path of Mira over

the past 30,000 years, with the features in the tail providing an unprecedented record of Mira's wind–ISM interaction over that period. No other such ultraviolet-emitting structure is known to be connected with an AGB star. The infrared detection mentioned previously is a bow shock observed around R Hydrae³, an AGB star at a greater distance (165 pc) and with a smaller space velocity (50 km s^{-1}). However, GALEX observations of R Hydrae show no ultraviolet emission associated with the infrared bow shock.

Although Mira has been extremely well studied at all wavelengths, the bow shock and tail have previously not been detected. We outline the three major morphological features in Fig. 1: the tail, the southern bow shock, and the southern and northern 'streams' that break up into individual knots (see Fig. 3 for details). The bow shock and knots show far-ultraviolet and near-ultraviolet emission. Remarkably, the tail has only far-ultraviolet emission. The only detectable near-ultraviolet emission in the tail region is associated with the northernmost knots. Typical far-ultraviolet surface brightnesses are 30.2 ± 0.15 , 28.0 ± 0.03 and 29.6 ± 0.1 AB magnitudes per arcsec² in the bow-shock, knot and near-tail regions, respectively. These show far-ultraviolet–near-ultraviolet colours of 0.0, -0.2 and < -3 , respectively. The far-ultraviolet luminosities for the bow shock, streams and tail are 7×10^{30} , 3×10^{31} and $7 \times 10^{31} \text{ erg s}^{-1}$, respectively, for a total far-ultraviolet luminosity of $\sim 10^{32} \text{ erg s}^{-1}$.

We have searched for counterparts of these features at other wavelengths. We obtained narrow-band H α images of the nebula with the Palomar 60-inch telescope. In these images only the knots show H α , with luminosities of $L_{\text{H}\alpha} \approx 2 \times 10^{29} \text{ erg s}^{-1}$. Images of the tail place an upper limit of $L_{\text{H}\alpha} < 10^{30} \text{ erg s}^{-1}$. There are no counterparts to the tail in optical, near- or far-infrared continua. Optical spectroscopy (Fig. 3) shows evidence that the knots are shocked and ionized by the post-bow-shock flow.

These observations suggest the following physical picture. Mira A produces a cool, molecular wind¹¹; the mass loss rate is $\dot{M} \approx 3 \times 10^{-7} M_{\odot} \text{ yr}^{-1}$ (where M_{\odot} is the solar mass) and the wind velocity is $v_w \approx 5 \text{ km s}^{-1}$. The wind is mildly anisotropic and shows evidence of a bipolar component¹². The space velocity of Mira AB through the ambient interstellar medium produces a bow shock with a termination shock standoff distance $l_0 \approx 1.6 \times 10^{17} \text{ cm}$. The preshock density obtained by balancing the ram pressures at the termination shock is $n_0 \approx 0.8 \text{ cm}^{-3}$. The resulting strong shock is non-radiative, because the post-shock gas at temperature $T_1 \approx (3/16k)mv_0^2 = 5 \times 10^5 \text{ K}$ (with k being the Boltzmann constant, m being the mass of Mira's wind, and v_0 being the space velocity of Mira) and density $n_1 \approx 6 \text{ cm}^{-3}$ has an isochoric cooling time¹³ of ~2,000 years. The rise and fall of ultraviolet emissivity tracks the monotonic increase in ionization level through C³⁺ to the dominant

¹Department of Physics, Math and Astronomy, California Institute of Technology, 1200 East California Boulevard, Mail Code 405-47, Pasadena, California 91125, USA. ²Observatories of the Carnegie Institution of Washington, 813 Santa Barbara Street, Pasadena, California 91101, USA. ³Department of Astronomy, Columbia University, New York, New York 10027, USA. ⁴Department of Physics and Astronomy, 430 Portola Plaza, UCLA, Los Angeles, California 90095-1547, USA. ⁵Space Sciences Laboratory, University of California, Berkeley, 7 Gauss Way, Berkeley, California 94720, USA.

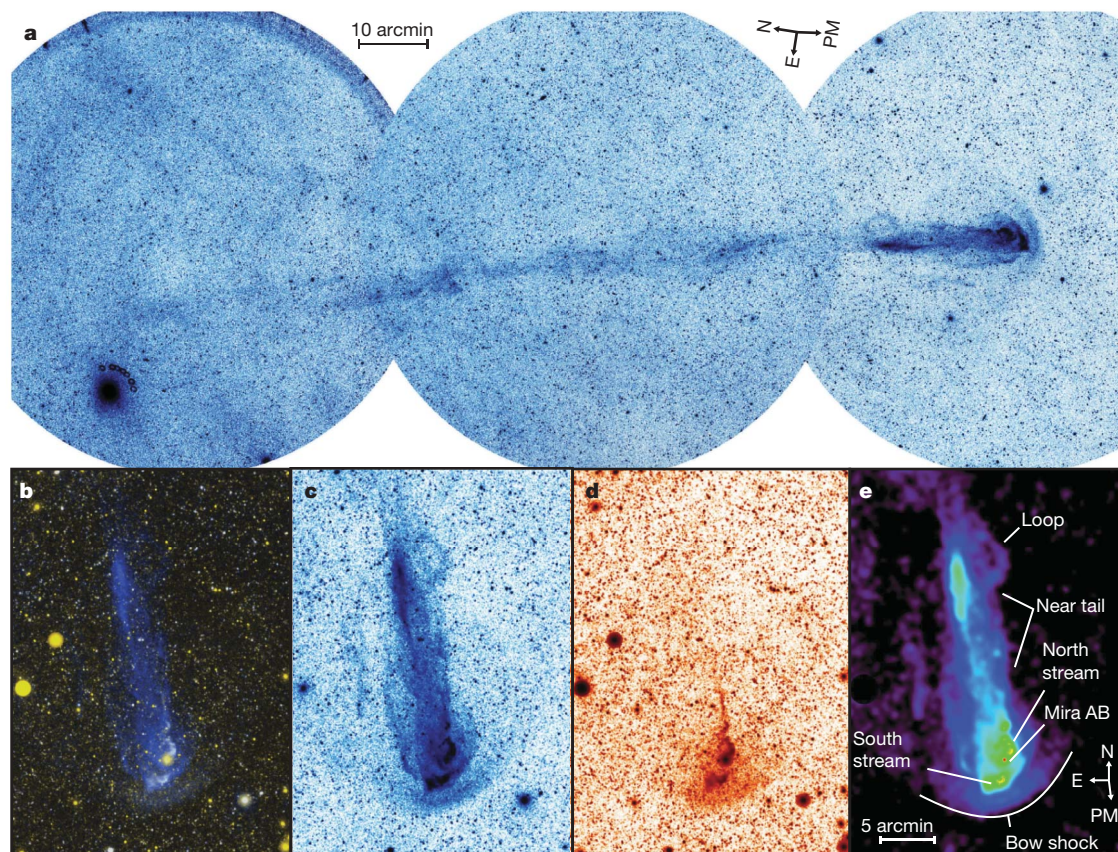


Figure 1 | Ultraviolet imaging of the Mira tail and bow shock. **a**, The far-ultraviolet (effective wavelength $\lambda_{\text{eff}} = 151.6$ nm; full-width at half-maximum, FWHM = 25.6 nm) mosaic of the Mira AB tail and bow shock. The data have been histogram equalized. The co-added mosaic consists of 31 observations covering 3 pointings with a total exposure time of 8.9, 11.2 and 11.5 ks (left to right). The images were taken between 18 November and 15 December 2006. The rectangular region is 2.7×1.1 degrees. The orientation (N, E) and measured proper motion (PM) vectors are indicated. The observed position angle of the tail is 194 degrees, in agreement with the observed proper motion vector once solar motion is accounted for. **b**, Energy-scaled colour

composite image. Far ultraviolet is blue; near ultraviolet ($\lambda_{\text{eff}} = 226.7$ nm; FWHM = 73.0 nm) is red; the average of the two ultraviolet bands is green. The region is 26×36 arcmin with an exposure time of 11.5 ks. North is up and east is left. The images were taken on 18–19 November 2006. **c**, **d**, The histogram-equalized far-ultraviolet (**c**) and near-ultraviolet (**d**) images covering the same physical region as **b**. There is a weak near-ultraviolet contribution to the bow shock and a complete lack of near-ultraviolet emission in the near-tail region. Each image has been boxcar-smoothed by 2 pixels (3 arcsec). **e**, This far-ultraviolet image has been enhanced by point source subtraction and adaptive smoothing.

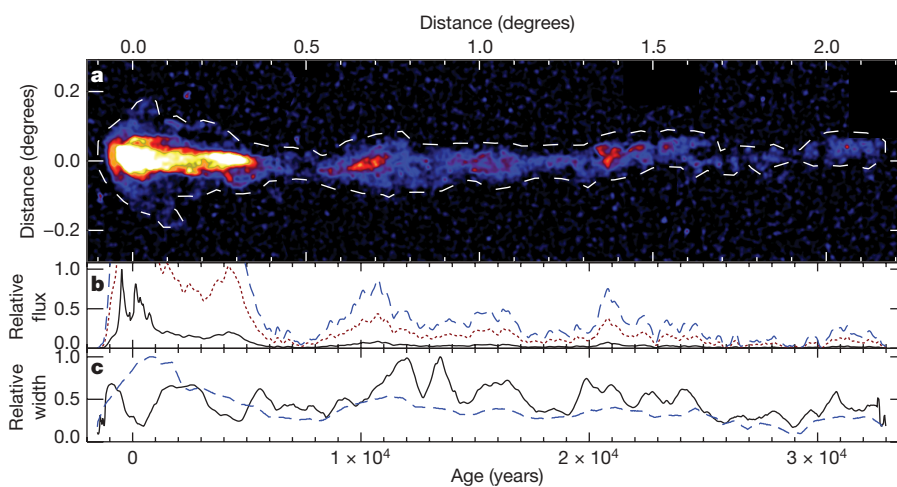


Figure 2 | 30,000-year history of Mira. **a**, Far-ultraviolet mosaic of the Mira AB tail extending more than 2 degrees. The image has been enhanced by point source subtraction and adaptive smoothing, has been rebinned by a factor of 4 into 6 arcsec pixels, and the background gradient has been subtracted. The dashed line is a total surface brightness contour of 31 AB magnitudes per arcsec². Mira AB is located at the origin (0,0). The images were taken between 18 November and 15 December 2006. **b**, Flux versus age. The solid black line is the relative flux within the surface brightness contour displayed in the top panel as a function of time, assuming a proper motion of

226 mas yr^{-1} . Zero age represents the current position of Mira AB. The dotted red line is the same multiplied by a factor of five, and the dashed blue line is the same multiplied by a factor of ten. The flux from Mira AB has been masked and is not included in the plotted flux. **c**, Width versus age. The solid black line is the relative FWHM within the surface brightness contour displayed in the top panel. The dashed blue line is the relative full width of the same contour. The time ordinate is the same as that of the middle panel. Mira AB has been masked.

C^{5+} at temperature T_1 . At the apex of the bow shock, the post-shock velocity in the Mira frame is $v_1 = 35 \text{ km s}^{-1}$. This rises with transverse position because of the conservation of the parallel velocity component across the oblique shock.

The shear flow of the hot post-shock gas past the cool wind will drag and decelerate the wind in the ISM frame. The knots have a higher density and thus more fully developed radiative shocks (Fig. 3). The position of the knots on a north–south axis is consistent with the bipolar component in Mira’s wind¹². The curvature of the southern stream of knots away from the north–south axis of the bipolar flow suggests deceleration by the post-shock flow. Knot A in the southern stream has yet to be decelerated and has the highest relative velocity. The upwind face of knot A between knot A and B is the only region showing [S II] emission. This is consistent with models of low-velocity shocks for Herbig–Harro objects¹⁴, which show a peak in [S II] emission near wind velocities of $\sim 40 \text{ km s}^{-1}$.

Most of Mira’s stellar wind is decelerated by viscous drag from the post-bow-shock flow. A central issue, therefore, is the source of the long-lived ultraviolet tail emission. It could be produced by dust scattering of interstellar light, molecular hydrogen emission, the hydrogen two-photon continuum, or coronal line emission from shocks or intermediate-temperature gas at $\sim 10^5 \text{ K}$. We have used

GALEX grism mode observations to constrain the spectrum of the emission. The details of this analysis are provided in Supplementary Information. Although AGB winds are dusty, dust-scattered far-ultraviolet emission is ruled out by a poor grism fit, the lack of observed near-ultraviolet emission, and the brightness of the emission in the absence of an illumination source other than the interstellar radiation field. The process providing the best fit to the grism image is H_2 emission. It also produces no detectable counterparts at other wavelengths. The far-ultraviolet emission cannot be fluorescence of H_2 excited by the ambient interstellar ultraviolet radiation field¹⁵ because this fails to produce the observed brightness by more than a factor of seven. Rather, we propose that the emission is excited collisionally¹⁶ by the interaction of H_2 in the cool wind wake with hot electrons in the post-shock gas resulting from the bow shock that also entrains and decelerates the wind. This is in accordance with the fact that the ultraviolet-emitting gas is likely to be cool, because the pressure of a hot gas would be much higher than the ambient ISM making it hard to maintain the narrow collimation, observed in Figs 1 and 2, for 30,000 years.

Indeed, this emission mechanism provides consistency between the global properties of the nebula and the transition rates expected from collisional excitation, and is consistent with a near equilibrium

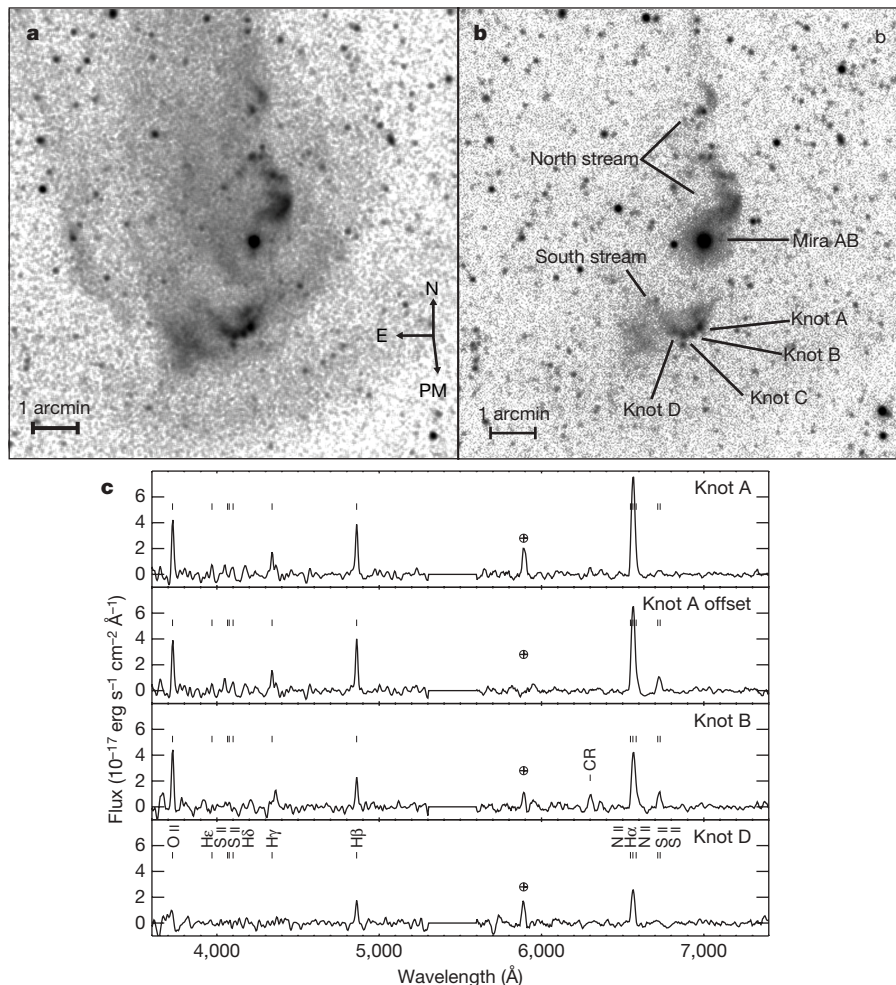


Figure 3 | Ultraviolet images and optical spectra of the streams and knots. **a, b**, The far-ultraviolet (**a**) and near-ultraviolet (**b**) images of the $10 \times 10 \text{ arcmin}^2$ region around Mira AB. North is up and east is left. **c**, The spectra were taken on 12 December 2006 with the Double Spectrograph on the Palomar 5-m telescope. The extractions were centred on the knots indicated, with the exception of the knot A offset, which was moved to coincide with the [S II] emission between knots A and B. The presence of the Balmer lines and the [O II] and [S II] lines is consistent with a low-velocity

secondary shock formed around each knot because the post-bow-shock flow affects the knots with a velocity of 35 km s^{-1} . This flow is slowing down the upstream velocity of each knot successively, thus causing the arc in their positions. The [S II] appearing at the leading edge of knot A is consistent with this picture because knot A would have the largest relative velocity with respect to the flow. The circled cross indicates night sky lines and CR indicates cosmic ray hits.

between dissociation and replenishment of H_2 from Mira's wind. At the interface of cool wind and hot post-shock gas, ~ 30 -eV electrons from the latter excite H_2 in the former into the $B^1\Sigma_g^+$ (Lyman) electronic level. The tail far-ultraviolet luminosity implies 5×10^{42} molecules s^{-1} are radiating. On the basis of the collisional excitation cross-sections into unbound states¹⁷, the dissociation rate will be half this, in rough equilibrium with the H_2 replenishment rate of $\sim 3 \times 10^{42}$ molecules s^{-1} from the predominantly molecular¹⁸ AGB wind with $\dot{M} \approx 3 \times 10^{-7} M_\odot yr^{-1}$. We assume that the average wind flux over the past $\sim 10^4$ years is similar to that measured at present. This ratio of photon emission to dissociation has also been observed in Herbig–Haro objects¹⁹. Collisional excitation, emission and dissociation would occur in the thin multiphase layer ($\sim 10^{15}$ – 10^{16} cm), with the total rate being the product of the electron velocity, electron density and interface area ($v_e n_e A$). Using the post-shock temperature and density, the implied interface area is $\sim (5 \times 10^{16})^2$ cm^2 , consistent with the nebular dimensions. Emission from a multiphase surface can produce a more complex morphology in the tail than volume emission, as is observed.

The total mechanical energy available to power the nebula is estimated by assuming that the local ISM brings the wind (again at the current mass flux) to rest from its space velocity of 130 $km s^{-1}$. The result, 2×10^{33} $erg s^{-1}$, is 20 times the observed far-ultraviolet luminosity.

Mira A is a thermally pulsing AGB star, and the wind flux may vary over the thermal pulse cycle²⁰. Signatures of thermal pulsation in AGB winds have previously been observed in the infrared²¹, but never before in the ultraviolet. Figure 2 illustrates the evidence for a cyclic behaviour in Mira's wind, with maxima falling roughly every $\sim 10^4$ years. A periodogram²² shows a highly significant peak around 10^4 years and a secondary peak at approximately half this value. The bottom panel of Fig. 2, plotting the wake width versus time, provides additional evidence for this periodic timescale. The standoff distance and characteristic radius of the wake, l_0 , vary with wind flux consistently with the expected $l_0 \propto \dot{M}^{1/2}$.

We can compare this timescale with that predicted from the thermal pulse theory. Mira's mass, derived from the well established period–mass–radius relationship²³ for long-period variable stars, is $\sim 1.5 M_\odot$. This mass is consistent with models predicting a thermal pulse cycle at least an order of magnitude longer²⁰ than the periodicity timescale in Mira's wake. The only thermal pulse models consistent with the observed wind wake periodic timescale have masses of $\sim 4 M_\odot$ (ref. 20). Alternatively, the periodic features could be density fluctuations caused by large-scale turbulence. Mira's cool wind has a high Reynolds number ($\sim 10^4$), and the wind wake may grow turbulent. The large loop on the west side of the tail could be a decaying turbulent vortex, as predicted by hydrodynamic simulations of AGB winds interacting with the ISM^{24,25}. Variations in the ISM density on parsec scales could provide another alternative explanation.

A deeper understanding of the Mira nebula requires detailed hydrodynamic and microphysical modelling. Ultra-deep optical and near-infrared observations may reveal the expected extremely faint H_2 emission lines, whereas far-infrared observations may uncover warm, entrained dust in the wake. Absorption-line observations of background stars in the H_2 Lyman and Werner bands would be extremely interesting, as would observations of low-ionization atomic species. The discovery of a two-degree-long wind wake emitting only in the far ultraviolet provides an unprecedented fossil record of post-main-sequence stellar evolution and mass loss, a laboratory for the study of astrophysical turbulence and the complex

physics of a multiphase hydrodynamical flow, and suggests a new cooling process for hot gas that entrains a cool molecular phase. After 400 years of study, Mira continues to astound.

Received 30 March; accepted 11 June 2007.

- Hoffleit, D. History of the discovery of Mira stars. *J. Am. Ass. Var. Star Observ.* **25**, 115–136 (1997).
- Schröder, K.-P. & Sedlmayr, E. The galactic mass injection from cool stellar winds of the 1 to $2.5 M_\odot$ stars in the solar neighbourhood. *Astron. Astrophys.* **366**, 913–922 (2001).
- Ueta, T. S. *et al.* Detection of a far-infrared bow shock nebula around R Hya: the first MIRIAD results. *Astrophys. J.* **648**, L39–L42 (2006).
- Prieur, J. L. *et al.* High angular resolution observations of late-type stars. *Astrophys. J.* **139**, 249–258 (2002).
- Karovska, M., Schlegel, E., Hack, W., Raymond, J. C. & Wood, B. E. A. Large X-ray outburst in Mira A. *Astrophys. J.* **623**, L137–L140 (2005).
- Ireland, M. J. *et al.* Born again protoplanetary disk around Mira B. *Astrophys. J.* **662**, 651–657 (2007).
- Martin, D. C. *et al.* The Galaxy Evolution Explorer: a space ultraviolet survey mission. *Astrophys. J.* **619**, L1–L4 (2005).
- Knapp, G. R., Pourbaix, D., Platais, I. & Jorissen, A. Reprocessing the Hipparcos data of evolved stars. III. Revised Hipparcos period–luminosity relationship for galactic long-period variable stars. *Astron. Astrophys.* **403**, 993–1002 (2003).
- Turon, C. *et al.* Version 2 of the Hipparcos Input Catalogue. *Bull. Inf. Centre Donnees Stell.* **43**, 5–6 (1993).
- Evans, D. S. The revision of the general catalog of radial velocities. *IAU Symp.* **30**, 57–62 (1967).
- Ryde, N., Gustafsson, B., Eriksson, K. & Hinkle, K. H. Mira's wind explored in scattering infrared CO lines. *Astrophys. J.* **545**, 945–956 (2000).
- Josselin, E. *et al.* Strong asymmetries in the neutral envelope of Mira. *Astron. Astrophys.* **362**, 255–262 (2000).
- Ferland, G. J. *et al.* CLOUDY 90: numerical simulation of plasmas and their spectra. *Publ. Astron. Soc. Pacif.* **110**, 761–778 (1998).
- Hartigan, P., Raymond, J. & Hartmann, L. Radiative bow shock models of Herbig–Haro objects. *Astrophys. J.* **316**, 323–348 (1987).
- Martin, C., Hurwitz, M. & Bowyer, S. Discovery of molecular hydrogen fluorescence in the diffuse interstellar medium. *Astrophys. J.* **354**, 220–228 (1990).
- Liu, W. & Dalgarno, A. The ultraviolet spectrum of the Jovian dayglow. *Astrophys. J.* **462**, 502–518 (1996).
- Khakoo, M. A., Trajimar, S., McAdams, R. & Shyn, T. W. Electron-impact excitation cross sections for the $b^3 \Sigma_u^+$ state of H_2 . *Phys. Rev. A* **35**, 2832–2837 (1987).
- Bowers, P. F. & Knapp, G. R. Detection of H I emission in the circumstellar envelope of Omicron Ceti (Mira). *Astrophys. J.* **332**, 299–304 (1988).
- Raymond, J. C., Blair, W. P. & Long, K. S. Hopkins ultraviolet telescope observations of H_2 emission lines from HH 2. *Astrophys. J.* **489**, 314–318 (1997).
- Vassiliadis, E. & Wood, P. R. Evolution of low- and intermediate-mass stars to the end of the asymptotic giant branch with mass loss. *Astrophys. J.* **413**, 641–657 (1993).
- Speck, A. K., Meixner, M. & Knapp, G. R. Discovery of parsec-sized dust shells around AFGL 2688 and AFGL 618. *Astrophys. J.* **545**, L145–L148 (2000).
- Scargle, J. D. Studies in astronomical time series analysis. II—Statistical aspects of spectral analysis of unevenly spaced data. *Astrophys. J.* **263**, 835–853 (1982).
- Wood, P. R. in *Miras to Planetary Nebulae: Which Path for Stellar Evolution?* (eds Mennessier, M. O. & Omont A.) 67–84 (Editions Frontieres, Gif-sur-Yvette, 1990).
- Wareing, C. J. *et al.* Detached shells as tracers of asymptotic giant branch–interstellar medium bow shocks. *Mon. Not. R. Astron. Soc.* **372**, L63–L67 (2006).
- Wareing, C. J., Zijlstra, A. A. & O'Brien, T. J. Vortices in the wakes of AGB stars. *Astrophys. J.* **660**, L129–L132 (2007).

Supplementary Information is linked to the online version of the paper at www.nature.com/nature.

Acknowledgements We thank B. Cenko, S. Browne, S. Kulkarni and F. Harrison for assistance in obtaining optical data, and M. Shara and P. Szkody for comments. This work was supported by the National Aeronautics and Space Administration.

Author Information Reprints and permissions information is available at www.nature.com/reprints. The authors declare no competing financial interests. Correspondence and requests for materials should be addressed to D.C.M. (cmartin@sr.caltech.edu).